ARCTIC
VOL. 61, NO. 3 (SEPTEMBER 2008) P. 243–254

Extending the Late Holocene Tephrochronology of the Central Kenai Peninsula, Alaska

RICHARD J. PAYNE[1,2] and JEFFREY J. BLACKFORD[2]

(*Received 4 January 2006; accepted in revised form 30 October 2007*)

ABSTRACT. Tephrochronology, the reconstruction of past volcanic ash deposition, provides a valuable method for dating sediments and determining long-term volcanic history. Tephra layers are highly numerous in Alaska, but knowledge of their occurrence and distribution is incomplete. This study expands the regional tephrochronology for the Kenai Peninsula of south-central Alaska by investigating the tephrostratigraphy of two peatland sites. We located seven visible tephras and seven microtephras and investigated the particle size and geochemistry of the visible tephras. Radiocarbon dates were used to estimate the timescale of each core. Geochemical comparison showed that the visible tephras originated from late Holocene eruptions of Augustine, Crater Peak–Mt. Spurr, and Hayes volcanoes. Some of the tephras had been documented previously, and these new findings expand their known range. Others represent eruptions not previously reported, including a Crater Peak–Mt. Spurr eruption around 430 cal. BP. The results provide new tephra data for the region, illustrate the spatial heterogeneity of tephra deposition, and show the potential of microtephras for expanding the regional tephra record.

Key words: tephra, cryptotephra, peatlands, Alaska, volcanoes, electron probe microanalysis

RÉSUMÉ. La téphrochronologie, soit la reconstruction d'anciens dépôts de cendres volcaniques, constitue une méthode valable pour dater les sédiments et déterminer l'historique des volcans à long terme. En Alaska, les couches de téphra sont nombreuses, mais on ne sait pas tout sur leur occurrence et leur répartition. Cette étude a permis d'approfondir la téphrochronologie régionale de la péninsule de Kenai du centre-sud de l'Alaska grâce à la téphrostratigraphie de deux tourbières. Nous avons repéré sept téphras visibles et sept microtéphras, puis nous avons examiné la taille des particules de même que la géochimie des téphras visibles. Les dates déterminées par le radiocarbone ont servi à estimer l'échelle de temps de chaque carotte. La comparaison géochimique a permis de constater que les téphras visibles remontent aux éruptions du Holocène supérieur des volcans Augustine, Crater Peak-Mt. Spurr et Hayes. Certains des téphras ont déjà été documentés, et ces nouvelles constatations permettent d'étendre leur aire d'extension connue. D'autres représentent des éruptions qui n'avaient jamais été signalées, dont l'éruption de Crater Peak-Mt. Spurr vers 430 cal. BP. Les résultats ont donné lieu à de nouvelles données relatives au téphra dans la région, en plus d'illustrer l'hétérogénéité spatiale des dépôts de téphra et de montrer que les microtéphras peuvent permettre de pousser plus loin les données régionales concernant le téphra.

Mots clés : téphra, cryptotéphra, tourbières, Alaska, volcans, analyse par microsonde électronique

Traduit pour la revue *Arctic* par Nicole Giguère.

INTRODUCTION

Preserved layers of tephra (volcanic ash) are valuable for reconstructing volcanic eruption histories, as isochrones for palaeo-environmental studies, and for investigating volcanic impacts on the environment. Alaska contains over 100 volcanoes active in the Quaternary, and tephrochronologies have been established in several areas, although many spatial and temporal gaps remain. The Kenai Peninsula of south-central Alaska is close to several Holocene-active volcanoes and has been subject to many historical ashfalls. The peninsula is one of the most densely populated areas in the state and is crossed by major international air routes, so even relatively modest eruptions can cause major impacts. The area is also the site of ongoing palaeoecological studies, which use tephra layers for dating and correlating sequences. Previous studies have identified tephras from several volcanic sources (Riehle, 1985; Begét et al., 1994; Combellick and Pinney, 1995), but an improved knowledge of the history and spatial dimensions of tephra deposition is needed for hazard assessment and chronological precision. Peatlands are effective at trapping and preserving tephra with minimal post-depositional movement or geochemical change over millennia, and even thin tephra layers in peat can be located, extracted, and identified (Dugmore et al., 1992, 1996; Payne et al., 2005). This study investigates the visible and microscopic tephrochronology of two peatlands in the Kenai Peninsula.

[1] Department of Geography, Queen Mary, University of London, Mile End Road, London E1 4NS, United Kingdom; r.j.payne@manchester.ac.uk
[2] Geography, School of Environment and Development, The University of Manchester, Oxford Road, Manchester, M13 9PL, United Kingdom

SITES AND METHODS

The two sites sampled were Sterling Mire, a kettle peatland on the Kenai Lowlands (60˚31′ N, 150˚31′ W), and Moose Pass peatland (60˚30′ N, 149˚26′ W; Fig. 1), located 60 km to the east in the Kenai Mountains (Payne et al., 2006). Cores were extracted from the deepest section of the sites using a Russian-pattern peat corer with a 50 mm bore (Aaby and Digerfeldt, 1986). Visible tephra layers were located and confirmed by microscopy. The particle size distribution of visible tephra layers was investigated using laser-diffraction particle size analysis (Beckman Coulter LS 13 320), with organic materials removed by acid digestion. In addition to visible tephra layers, we also identified non-visible microtephra layers (also termed cryptotephras: Lowe and Hunt, 2001) using a simplified ashing method (Pilcher and Hall, 1992). Subsamples 10 mm thick extracted from the core were incinerated at 550˚C, and the inorganic residue was mixed with glycerol on a microscope slide. Loss on ignition (LOI) was calculated from pre- and post-incineration weights. Tephra shards were identified under the microscope by their distinctive angular and vesicular morphology; no material remained for geochemical analyses. Location of tephra layers was complicated by the high proportion of other mineral material in the peat, particularly lower in the cores, where diatom frustules were often numerous. Isolated tephra shards were present in several of the samples, but only distinct microtephra layers with abundant tephra shards are presented here.

One aim of this study was to provide additional comparison data for microtephra studies elsewhere in Alaska. We based correlations between tephras solely on major element glass geochemistry. While this approach may disregard other sample characteristics, these are rarely useful for microtephra correlation, and many studies (e.g., Begét et al., 1994; Hunt, 2004) have demonstrated that useful correlations can be made on the basis of glass geochemistry alone. The glass geochemistry of the visible tephra layers was determined using wavelength dispersive electron probe microanalysis (EPMA), the standard technique used in most tephra studies. EPMA can produce results that are precise and replicable between analysis centres. Although discrepancies may arise from differences in probe set-up and operation, these are minimized when the probe is well calibrated (Hunt and Hill, 1993; Hunt et al., 1998).

Tephra shards were extracted using acid digestion, following the methods of Persson (1971) and Dugmore (1989), which have been used in numerous tephra studies and are considered reliable (Dugmore et al., 1992). A recent study (Blockley et al., 2005) demonstrated notable cation leaching; however, while such leaching is possible in this study, it is likely to be of limited extent and may be further reduced through sample polishing. Samples with a 'B' notation (Table 1) were analyzed with an ARL-SEMQ microprobe at the Department of Earth Science, University of Bergen, using 15 kV accelerating voltage, 10 nA beam current, and a 1 mm beam diameter. Samples with an 'E' notation were analyzed on a Cameca SX100 microprobe at the School of Geosciences, University of Edinburgh, with 20 kV accelerating voltage and a 4 nA beam current. The beam was rastered over a 10 × 10 mm grid to minimize sodium mobilization. Microprobe choice was dictated by logistical considerations and does not reflect any intrinsic difference between the two sets of samples. Analyses with oxide totals under 95% were excluded following Hunt and Hill (1993).

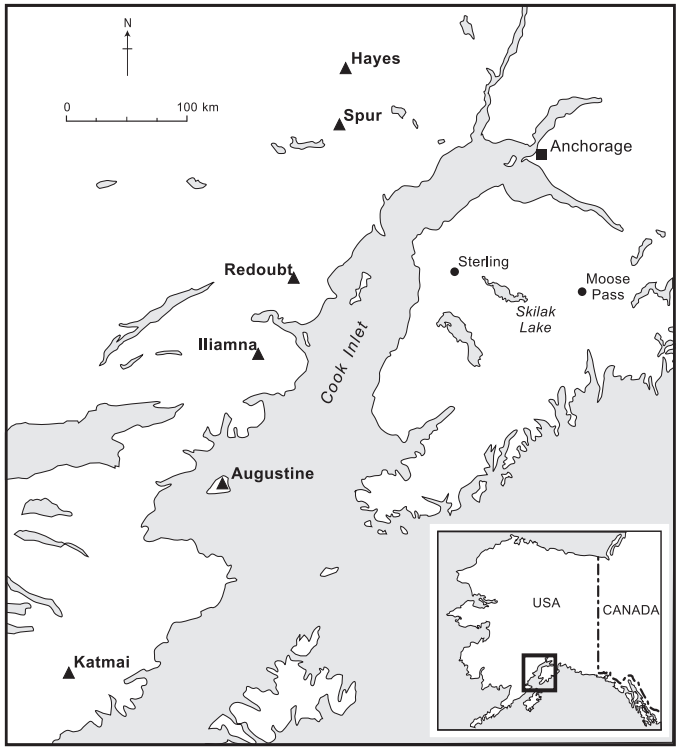

FIG. 1. Location map of Moose Pass and Sterling Mire sites (●) and selected volcanoes (▲). Also shown is Skilak Lake, a nearby site of previous research.

To determine the source of the tephras, we compared the glass geochemical data to a large data set compiled from previously published studies of tephra in southern Alaska (Downes, 1985; Riehle, 1985; Riehle et al., 1987, 1990, 1992, 1999 (selected data); Begét et al., 1991, 1992; Richter et al., 1995; Begét and Motyka, 1998; Child et al., 1998). Previous studies have used different electron microprobe centres and adopted a variety of analytical conditions, and these differences may complicate data comparisons.

Correlations between glass geochemical data from tephras in this study and those from previous studies were investigated using a variety of techniques. We constructed plots of absolute and relative oxide abundance and calculated similarity coefficients, using both the conventional similarity coefficient (SC) and the computationally more intensive weighted SIMAN coefficient. The SC is calculated as:

$$SC_{(A,B)} = \frac{\sum_{i=1}^{n} R_i}{n}$$

where i = element number, n = number of elements, and $R_i = X_{iA}/X_{iB}$ (if $X_{iA} < X_{iB}$) or X_{iB}/X_{iA}, (if $X_{iB} < X_{iA}$). (X_{iA} and X_{iB} = the concentration of element i in samples A and B.) Oxides with an SC less than 0.4% were excluded from the calculation (Borchardt et al., 1972; Riehle, 1985). The conventional similarity coefficient was applied to test the correlation between all tephras in this study and all comparison data. Where the SC indicated a reasonable degree of similarity (SC >≈ 0.90), we calculated weighted SIMAN coefficients that weight each oxide according to its analytical precision. The SIMAN coefficient is calculated as:

$$SIMAN_{(A,B)} = \frac{\sum_{i=1}^{n} R_i g_i}{\sum_{i=1}^{n} g_i} \qquad g_i = 1 - \sqrt{\frac{(\sigma_{iA}/X_{iA})^2 + (\sigma_{iB}/X_{iB})^2}{E}}$$

where σ_{iA} = 1 standard deviation for X_{iA}, E is the relative error due to the detection limit (set here at 0.7 to exclude only MnO from analysis), and g_i is the weighting factor. A SIMAN coefficient of 1 would indicate identical composition; however, given sample heterogeneity, this result is extremely unlikely. There is no unambiguous level that can be taken to indicate correlation; most studies adopt a value between 0.93 and 0.95 (Riehle, 1985; Carson et al., 2002). To help assess the value indicating correlation in this study, we randomly divided the data for each tephra into three subsets and calculated similarity coefficients (cf. Rodbell et al., 2002). Similarity coefficients are a rapid and computationally simple index of similarity between data averages, but they are not a rigorous statistical technique. Results need to be interpreted with caution, and potential correlations should also be evaluated using other techniques.

Radiocarbon dating was used to estimate the age of the tephra layers identified. Dates were obtained using conventional radiometric analysis on bulk peat samples from near the position of a visible tephra. Dates were calibrated using OxCal version 3.10 (Bronk Ramsey, 2005). The age of tephras that were not directly dated was estimated by linear interpolation from the calibrated date. Although peat accumulation may be modified by allogenic processes such as climate change or fire, numerous well-dated palaeoecological records show approximately linear accumulation rates over longer time scales (e.g., Aaby and Tauber, 1975). The age of one tephra (ST68) is more uncertain, as it lies below the dated horizon in this site.

RESULTS

Four visible tephras and three microtephra layers were detected in the Sterling site, and three visible tephras and four microtephra layers in the Moose Pass site (Fig. 2). Tephras are named by their site code (ST or MP) and the depth (cm) at which they occur: for example, the MP 10 tephra is at 10 cm below the surface in the Moose Pass site.

The loss on ignition results (Fig. 2) highlight the location and extent of the visible tephra layers; however, the majority of the microtephras do not show up in these plots. Lower LOI values near the base of the cores represent the transition towards ombrotrophy. Distinct loss on ignition troughs that are not associated with tephra layers, such as at 115 cm in Moose Pass, probably represent flood events.

Glass geochemical data are presented in Table 1. Any difference between performance of the two microprobes can be assessed by comparing results from tephras analyzed at both centres. For the MP 39 and MP 10a tephras, the data are broadly similar and coefficients are high (SIMAN = 0.96 and 0.95 respectively). Most of the difference can be accounted for by lower sodium totals in the Bergen data, which are probably due to the use of a static, focused beam. The data for MP 10b show greater difference, with a SIMAN coefficient of only 0.81 and major differences in several oxide means. Real heterogeneity in tephra composition and the small number of shards analyzed at Bergen may largely account for this difference.

To test the maximum achievable similarity coefficients, we divided the data sets in this study into three groups and calculated similarity coefficients. Results gave a mean SIMAN of 0.94 (σ 0.04). However, as these divided data sets are small, the oxide means will be less well characterized and coefficients may be underestimated. It therefore seems reasonable to apply a slightly higher limit. We adopted the 0.95 criterion applied in numerous previous studies. Lower SCs (over approximately 0.90) could indicate a different tephra from the same source (Riehle, 1985).

The peat cores were dated using radiocarbon dates on two peat samples. A radiocarbon date of 510 ± 100 BP (lab. code Gd-15806) was obtained from 40 to 50 cm in the Moose Pass site. This calibrates to 670–420 cal. BP (1 σ age range), giving an accumulation rate of approximately 13 yr cm^{-1}. A radiocarbon date of 850 ± 65 BP (lab. code URCRM-1273) was obtained from 35 to 40 cm in the Sterling Mire site. This calibrates to 920–670 cal. BP, giving an accumulation rate of approximately 23 yr cm^{-1}. These accumulation rates are within the range that would be expected of a poor fen and ombrotrophic mire in this region (Robinson and Moore, 1999).

Moose Pass

The MP 10 tephra is a 10 mm thick zone of mixed-size tephra with particle size peaks at 30 and 450 mm. The particle size may be less well characterized for this tephra than for the other layers because analysis was based on a smaller sample. The glass geochemical data show two populations; population MP 10a is more silicic (over 73% SiO_2 normalized) than population MP 10b (under 71% SiO_2; Table 1). It is possible that the two populations

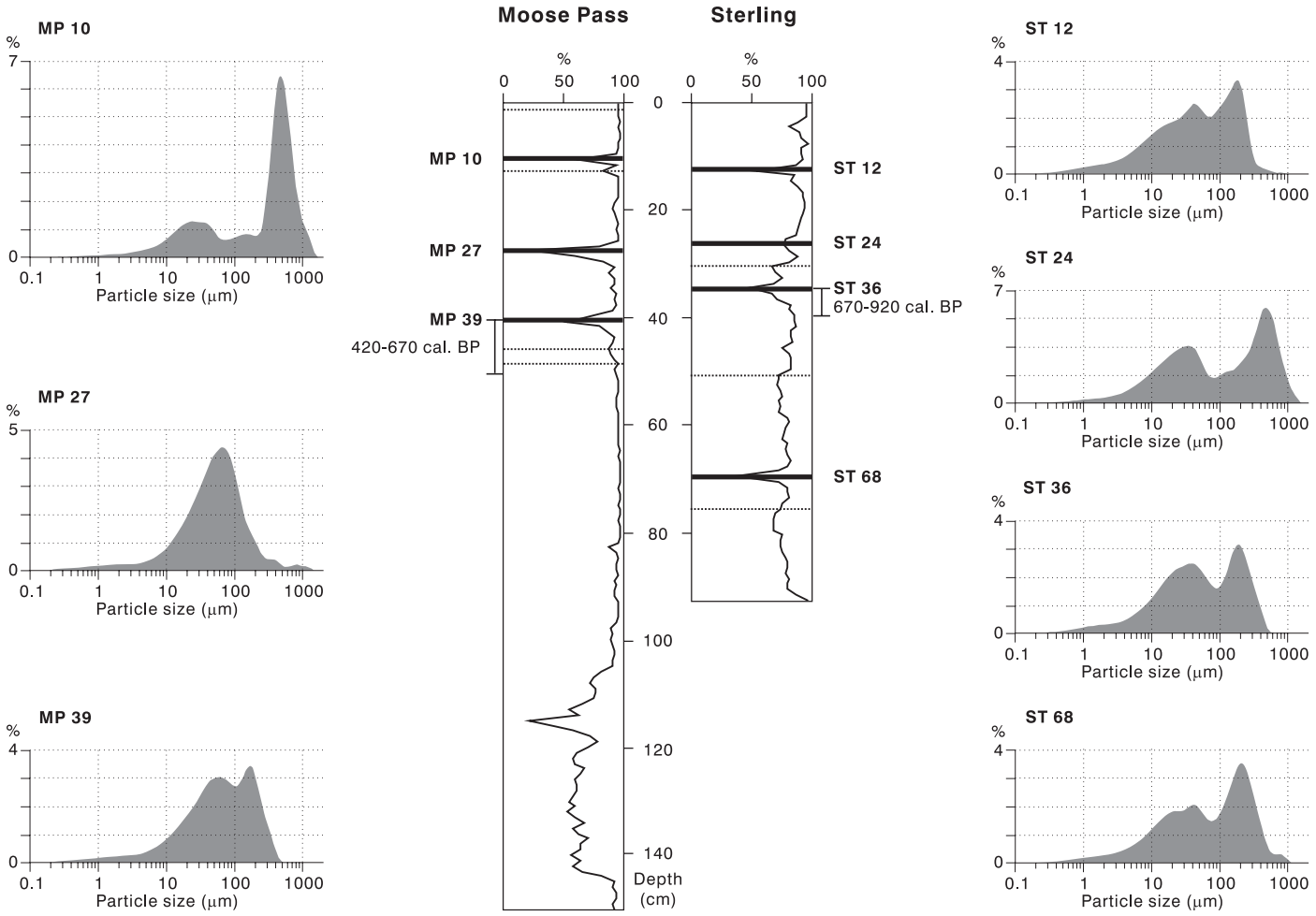

FIG. 2. Tephrostratigraphy of peat cores from the Moose Pass and Sterling peatlands. Central plots show loss on ignition (%), position of layers of visible tephras (solid horizontal lines) and microtephras (dotted lines). Horizontal variability in tephra depth has led to minor differences between the depth for which a tephra is named and the position of that tephra in these profiles. Peripheral plots show particle size profiles of visible tephra layers. The particle size analysis for the MP 10 tephra was based on a small sample and may not be adequately characterized.

represent separate but nearly contemporaneous eruptions, so each was compared separately to the other data. In comparison to the other layers in this study, the MP 10a population bears some similarity to ST 24 (SIMAN = 0.93), while the MP 10b population is more distinct (SIMAN ≤ 0.85). In comparison to results of previous studies, the MP 10a population bears a high degree of similarity to Augustine 1883 tephra (SIMAN ≤ 0.98: Begét et al., 1994; Fig. 3). The data show some difference from most Augustine tephra in Figure 4a, but are very similar to analyses of Augustine 1883 tephra (Figs. 3 and 4). The MP 10b population bears little similarity to any of the comparative data and is distinctly separate from any of the other tephras analysed (Fig. 4).

The MP 27 tephra, a layer 7 mm thick, is the only tephra in this study to show a monomodal particle size distribution centred on 65 mm. Glass geochemical data show a similarity to the MP 39 layer (SIMAN = 0.96). In comparison to data from previous studies, MP 27 shows a very high degree of similarity to tephra from Crater Peak–Mt. Spurr (Fig. 4) and particularly to data from a c. 300 BP eruption found at Skilak Lake (Fig. 3; SIMAN ≤ 0.98: Begét et al., 1994).

The MP 39 tephra is a 4 mm thick layer of tephra particles with a size distribution centred on 60 and 175 mm. Geochemical data show a heterogeneous composition without distinct populations. As in the similar MP 27 layer, the highest degree of similarity is with the c. 300 BP Crater Peak–Mt. Spurr tephra (Fig. 3: Begét et al., 1994), although the similarity coefficients are marginally lower (SIMAN ≤ 0.97).

Sterling Mire

The ST 12 tephra is a 2 mm thick layer with particle size peaks at 45 and 180 mm. Glass geochemical data show limited similarity to other data sets in this study (SIMAN ≤ 0.89). In comparison to data from previous studies, the greatest similarity is to data from Augustine Volcano, particularly the c. 500 BP Augustine ‘B’ tephra (Fig. 4; Begét et al., 1994). Similarity coefficients for the ST 12 tephra (SIMAN ≤ 0.92) are below the level required to indicate correlation, but still indicate a degree of glass geochemical similarity, as shown in Figure 3.

TABLE 1. Electron microprobe microanalysis (EPMA) results for glass shards from seven visible tephra layers in this study, along with the most similar comparison data from previous studies. Normalized data from all (N) analyses of each sample are based on eight major oxides. (Where manganese and chlorine oxides were analyzed, they were excluded from the analysis.) Analyses with oxide totals under 95% are not included, following Hunt and Hill (1993). For details, see Methods section. Full (non-normalized) data are presented in the Appendix.

Tephra Sample (This Study)	Comparison Data and Reference	Microprobe Used in This Study[1]	N	Estimated Date of Deposition (AD)[2]	SiO_2	TiO_2	Al_2O_3	FeO^3	MgO	CaO	Na_2O	K_2O	Similarity Coefficient[4]	SIMAN Coefficient[4]
ST12		E	30	1740	76.30	0.36	12.70	1.96	0.42	2.01	4.07	2.18		
	Augustine 'B' (A88-7-1; Begét et al., 1994)				75.73	0.39	13.04	2.08	0.49	2.29	3.97	2.01	0.92	0.92
	Augustine 'B' (SK11-3-18; Begét et al., 1994)				75.46	0.41	13.20	2.14	0.52	2.38	3.98	1.90	0.90	0.91
ST24		E	14	1480	76.89	0.30	12.66	1.48	0.32	1.47	3.84	3.02		
	Katmai 1912 (SK7-3-3p2; Begét et al., 1994)				77.23	0.32	12.38	1.64	0.27	1.27	4.01	2.87	0.93	0.94
	Katmai 1912 (SK7-4-3p2; Begét et al., 1994)				77.18	0.33	12.45	1.59	0.25	1.23	3.98	2.98	0.92	0.94
	Augustine 1883 (SK11-3-5; Begét et al., 1994)				75.06	0.32	13.77	1.65	0.40	1.71	4.04	3.04	0.92	0.93
ST36		E	16	1230	75.12	0.50	13.36	2.34	0.58	2.62	3.46	2.03		
	Augustine 'B' (SK7-4-11; Begét et al., 1994)				75.56	0.50	13.09	2.13	0.41	2.37	3.96	1.96	0.92	0.92
ST68		E	13	550	74.99	0.21	14.14	1.38	0.45	2.28	3.83	2.70		
	Hayes (A-T1; Comebellick and Pinney, 1994)				75.41	0.22	13.77	1.56	0.45	2.17	3.85	2.56	0.96	0.97
	Hayes (B-T1; Comebellick and Pinney, 1994)				75.72	0.23	13.53	1.44	0.40	2.17	3.97	2.53	0.95	0.96
MP10a		B/E	17	1875	75.70	0.32	13.55	1.67	0.39	1.74	3.62	3.00		
	Augustine 1883 (SK11-3-5; Begét et al., 1994)				75.06	0.32	13.77	1.65	0.40	1.71	4.04	3.04	0.97	0.98
	Augustine 1883 (SK11-2-5; Begét et al., 1994)				75.12	0.32	13.61	1.65	0.39	1.76	4.19	2.96	0.98	0.98
MP10b		B/E	22	1875	69.23	0.52	15.56	3.64	1.49	3.33	3.77	2.46		
MP27		B	11	1670	59.84	1.15	16.50	7.83	2.78	6.27	4.00	1.63		
	Crater Peak c. 300 BP (SK7-3-9; Begét et al., 1994)				59.74	1.18	16.24	7.74	2.84	6.27	4.30	1.69	0.98	0.98
	Crater Peak c. 300 BP (SK7-4-8; Begét et al., 1994)				59.44	1.19	16.24	8.02	2.87	6.49	4.12	1.63	0.98	0.98
MP39		B/E	59	1520	60.60	1.14	16.05	7.57	2.68	5.95	4.22	1.79		
	Crater Peak c. 300 BP (SK7-3-9; Begét et al., 1994)				59.74	1.18	16.24	7.74	2.84	6.27	4.30	1.69	0.97	0.97
	Crater Peak c. 300 BP (SK7-4-8; Begét et al., 1994)				59.44	1.19	16.24	8.02	2.87	6.49	4.12	1.63	0.95	0.95

[1] B = Bergen, E = Edinburgh, B/E = sample analyzed at both centres.

[2] Age estimates are based on linear interpolation from calibrated radiocarbon dates.

[3] Total Fe is reported as FeO.

[4] Similarity coefficients and SIMAN coefficients are calculated following Borchardt et al. (1972) and Borchardt (1974).

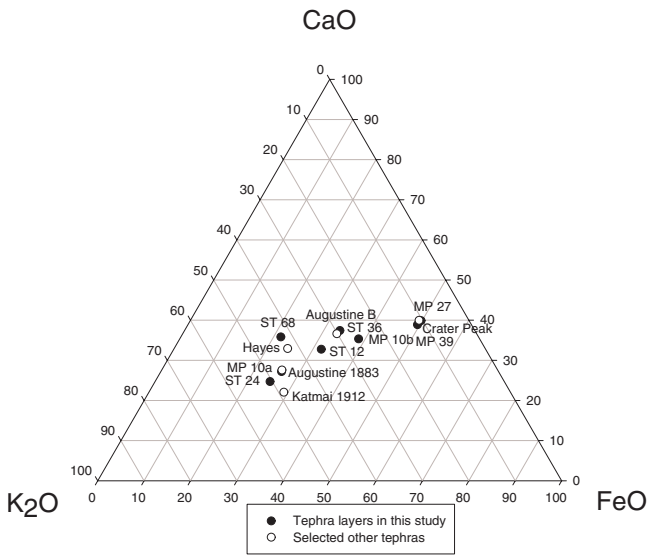

FIG. 3.Tri-plot of K_2O, FeO, and CaO, showing relative composition of tephra populations in this study and selected reference data (Riehle et al., 1990; Begét et al., 1994).

The ST 24 tephra is a 5 mm thick zone of particles with a bimodal size distribution centred on 35 and 490 mm. The data bear some similarity to comparison data, particularly the Katmai 1912 tephra (SIMAN ≤ 0.94) and the Augustine 1883 tephra (SIMAN ≤ 0.93; Fig. 3; Begét et al., 1994).

The ST 36 tephra is a 4 mm thick layer with particle size peaks at 35 and 175 mm. Glass geochemistry bears little similarity to other tephras in this study (SIMAN ≤ 0.87). Compared to data from previous studies the greatest similarity is to Augustine tephra (Fig. 4). Similarity coefficients indicate the greatest similarity with the c. 500 BP Augustine 'B' tephra (SIMAN ≤ 0.92; Begét et al., 1994).

The ST 68 tephra is a 3 mm thick layer with particle size distribution centred on 40 and 215 mm. The tephra has little geochemical similarity to other layers in this study (SIMAN ≤ 0.89). In comparison to data from previous studies, it is most similar to Hayes tephra found in interior Alaska (SIMAN ≤ 0.95: Begét et al., 1991) and the eastern Kenai Peninsula (Fig. 4; SIMAN ≤ 0.97: Combellick and Pinney, 1995).

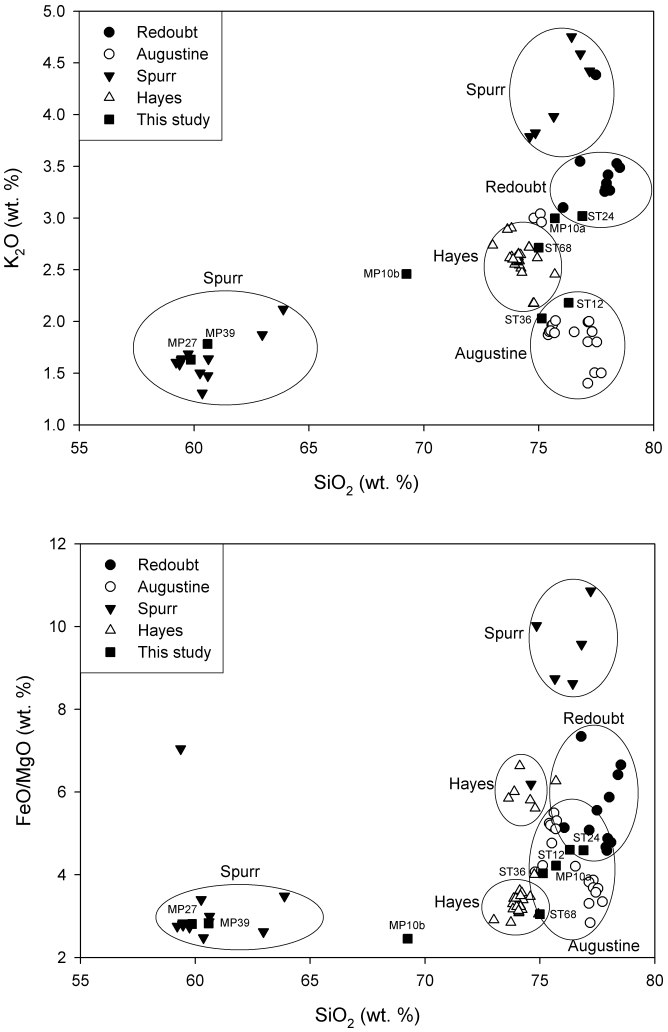

FIG. 4. Absolute abundance of selected major oxides in tephras analyzed in this study and selected reference data, with approximate fields enclosing the reference data.

DISCUSSION

The MP 10 tephra shows a high degree of similarity to the Augustine 1883 tephra. Given the estimated age of this tephra and the large magnitude of the eruption, the Augustine tephra seems a very probable source (Table 1). Both the MP 27 and MP 39 tephras bear a high degree of similarity to tephra from Crater Peak–Mt. Spurr. Begét et al. (1994) located a Crater Peak tephra dated to c. 300 BP, as well as an older layer (> 500 BP) that bears little geochemical similarity to MP 27 and MP 39. Despite the similarity in glass geochemistry, it is extremely unlikely that MP27 and MP39 are both the same tephra. Microscopy demonstrated both tephras to be well confined. Although some tephra shards may move down through peat (Payne et al., 2005), significant vertical movement of entire tephra layers in peatlands has never been demonstrated or seriously suggested. The Moose Pass mire receives all its moisture and nutrients from the atmosphere, so it is very unlikely for tephra to have been re-deposited at the site more than a hundred years after the original eruption. Linear extrapolation from the radiocarbon date suggests that the MP 27 tephra dates to c. 280 cal. BP and the MP39 tephra to c. 430 cal. BP. Given these estimated ages and the greater glass geochemical similarity, it seems probable that the MP 27 tephra is the c. 300 BP layer and the MP 39 tephra is from a previously unidentified eruption.

The source of the Sterling tephras is more complex to determine. The ST 12 tephra shows the greatest similarity to Augustine tephras; linear extrapolation from the radiocarbon date suggests an age of c. 210 cal. BP. The recorded Augustine eruption closest to this date is c. 300 BP (Smithsonian volcano database, www.volcano.si.edu). This eruption is the most likely candidate for ST 12. The ST 24 tephra shows greatest similarity to the Katmai-Novarupta 1912 tephra, but the age estimate of c. 470 cal. BP is

significantly too old. Glass geochemistry also shows some degree of similarity to Augustine tephras, but the data are inconclusive, and correlation cannot be reliably determined. The ST 36 tephra shows the greatest similarity to Augustine tephras and is directly dated to c. 720 cal. BP. An Augustine eruption dated to c. 750 BP is in close agreement with this age and provides the most probable source. The ST 68 tephra shows the greatest similarity to tephra from Hayes Volcano. Extrapolation from the radiocarbon date suggests an age of c. 1400 cal. BP, but there are no Hayes eruptions recorded between c. 3500 and c. 750 BP (Begét et al., 1991). However, this age estimate is poorly constrained, relying on the assumption of a constant accumulation rate below the dated horizon. Although there is no obvious change in stratigraphy lower in the core, it is possible that the accumulation rate may have changed as the mire developed towards ombrotrophy and older sediments became compressed. It is therefore conceivable that the tephra may represent one of the large Hayes eruptions from 4400 to 3600 BP (Riehle et al., 1990; Begét et al., 1991). In the absence of geochemical data, it is not possible to determine the source of the microscopic tephras; however, the likely age of the layer suggests that the tephra at 2.5 cm depth in the Moose Pass site probably represents one of the 1992 eruptions of Crater Peak–Mt. Spurr, the 1989–90 Redoubt eruption, or the 1986 Augustine eruption. Further microscopic tephras are dated to approximately 590, 1060, and 1570 cal. BP at Sterling Mire and approximately 100, 510, and 550 cal. BP at Moose Pass.

These results show several interesting features of the regional tephrochronology. Although some tephras have been previously documented in the region (MP 10, MP 27), many do not have obvious correlates. The MP 39 tephra is probably from a previously unrecognized eruption, while the ST 68 tephra may extend the distribution of Hayes tephra farther east across the Kenai Peninsula. Although the sources of all the tephras have not been conclusively ascertained, many appear to originate from Augustine Volcano, which is consistent with the high eruptive frequency of this volcano. Interestingly, none of the identified tephras appear to be from Redoubt Volcano despite its proximity and the frequent eruptions at this volcano (Begét and Nye, 1994).

A possible cause of the poor comparability with previous studies may be differences in electron microprobe performance. Although EPMA data are generally comparable between different centres, inter-laboratory comparison exercises have shown some exceptions to this. In particular, Hunt et al. (1998) showed that analyses by the USGS Menlo Park facility had lower sodium totals than other laboratories, including the Edinburgh centre used for some analyses in this study. The Menlo Park probe was used in the study of Riehle (1985). If sodium mobilization occurred in the analyses of Riehle (1985), the lower sodium totals may have complicated comparisons with the data presented here.

The frequency of microscopic tephras at these sites equals that of visible layers, which suggests that reliance on visible tephras may lead to underestimating the eruptive frequency of proximal volcanoes. Alternatively, the thinner layers may represent more distant eruptive sources. At sites nearer the source, a higher percentage of tephras may be recorded both in total and in visible form. Farther away, only microtephras may be found (Hall and Pilcher, 2002; Payne and Blackford, 2004). This study suggests that a combined approach that uses distal and proximal sites and includes microtephras would be most effective in reconstructing the frequency and magnitude of past events. Although these microtephra layers have not been identified to source, they are still important, as they show the relatively high frequency of smaller tephra-fall events, which may still be capable of environmental impacts (e.g., Blackford et al., 1992).

The results presented here highlight the spatial heterogeneity of tephra deposition on the Kenai Peninsula. The two sites in this study are only 60 km apart and cover similar time periods, but apparently none of the visible tephras are present at both sites. It is particularly notable that the Crater Peak–Mt. Spurr tephras in the Moose Pass site are not present in the Sterling Mire site, which is located almost directly between Moose Pass and the volcano. The Skilak Lake site investigated by Begét et al. (1994) is within 15 km of Sterling Mire; however, it seems that none of the tephras identified are common to both sites (Fig. 1). These differences are probably due to the prevailing meteorological conditions at the time of eruption and may represent palaeo-rainfall or snow cover patterns. Further work on the microtephras may improve these inter-site correlations.

Particle size analysis might allow tephras to be characterized by their particle size profiles and may be used to illustrate changing particle size with increasing distance from source. Comparison of particle size was not possible in this study because of the difference in tephra records between the two sites, but the approach merits future work. The tephra records appear to show that tephra deposition at these sites has been more frequent over the last 700 years than in earlier periods covered by these peat cores. In the case of microscopic tephras, this result may reflect the increasing difficulty of locating tephra layers deeper in the cores; however, for the visible tephras this seems to be a genuine result. Overall, the data presented here will aid the use of tephrochronology for hazard assessment and for dating palaeoenvironmental records from the region.

ACKNOWLEDGEMENTS

This research was carried out during the course of a Westfield studentship at Queen Mary, University of London and an EU Marie Curie doctoral fellowship at the University of Bergen. Fieldwork funding was provided by the Royal Society, the Bill Bishop Memorial

Trust, the Dudley Stamp Memorial Fund, and the Knowle Hill School Fund. Use of the Edinburgh microprobe was funded by the Natural Environment Research Council. Thanks to Peter Hill, Anthony Newton, Ole Tumyr, and Haflidi Haflidason for microprobe assistance and to Graham Bowden and Ed Oliver for preparing the map. Thanks to four anonymous reviewers for valuable comments on the manuscript.

REFERENCES

AABY, B., and DIGERFELDT, G. 1986. Sampling techniques for lakes and bogs. In: Berglund, B., ed. Handbook of Holocene palaeoecology and palaeohydrology. Chichester: Wiley. 181–194.

AABY, B., and TAUBER, H. 1975. Rates of peat formation in relation to degree of humification and local environment, as shown by studies of a raised bog in Denmark. Boreas 4:1–15.

BEGÉT, J.E., and MOTYKA, R.J. 1998. New dates of late Pleistocene dacitic tephra from the Mount Edgecumbe volcanic field, southeastern Alaska. Quaternary Research 49:123–125.

BEGÉT, J.E., and NYE, C.J. 1994. Postglacial eruption history of Redoubt Volcano, Alaska. Journal of Volcanology and Geothermal Research 62:31–54.

BEGÉT, J.E., REGER, R.D., PINNEY, D., GILLISPIE, T., and CAMPBELL, K. 1991. Correlation of the Holocene Jarvis Creek, Tangle Lakes, Cantwell and Hayes tephras in south-central and central Alaska. Quaternary Research 35:174–189.

BEGÉT, J.E., MASON, O., and ANDERSON, P. 1992. Age, extent and climatic significance of the c. 3400 BP Aniakchak tephra, western Alaska, USA. The Holocene 2:51–56.

BEGÉT, J.E., STIHLER, S.D., and STONE, D.B. 1994. A 500-year-long record of tephra falls from Redoubt volcano and other volcanoes in upper Cook Inlet, Alaska. Journal of Volcanology and Geothermal Research 62:55–67.

BLACKFORD, J.J., EDWARDS, K.J., DUGMORE, A.J., COOK, G.T., and BUCKLAND, P.C. 1992. Icelandic volcanic ash and mid-Holocene Scots pine (*Pinus sylvestris*) pollen decline in northern Scotland. The Holocene 2:260–265, doi:10.1177/095968369200200308.

BLOCKLEY, S.P.E., PYNE-O'DONNELL, S.D.F., LOWE, J.J., MATTHEWS, I.P., STONE, A., POLLARD, A.M., TURNEY, C.S.M., and MOLYNEUX, E.G. 2005. A new and less destructive laboratory procedure for the physical separation of distal glass tephra shards from sediments. Quaternary Science Reviews 24:1952–1960.

BORCHARDT, G.A., ARUSCAVAGE, P.J., and MILLARD, H.T. 1972. Correlation of the Bishop ash, a Pleistocene marker bed, using instrumental neutron activation analysis. Journal of Sedimentary Petrology 42:301–306.

BRONK RAMSEY, C. 2005. OxCal program v.3.10. Oxford: Oxford University.

CARSON, E., FOURNELL, J.H., MILLER, T.P., and MICKELSON, D.M. 2002. Holocene tephrochronology of the Cold Bay area, southwest Alaska Peninsula. Quaternary Science Reviews 21:2213–2228.

CHILD, J.K., BEGÉT, J.E., and WERNER, A. 1998. Three Holocene tephras identified in lacustrine sediment cores from the Wonder Lake area, Denali National Park and Preserve, Alaska, U.S.A. Arctic and Alpine Research 30:89–95.

COMBELLICK, R.A., and PINNEY, D.S. 1995. Radiocarbon age of probable Hayes tephra, Kenai Peninsula, Alaska. In: Combellick, R.A., and Tannian, F., eds. Short notes on Alaska geology 1995. Professional Report 0117. Fairbanks: Alaska Division of Geological & Geophysical Surveys. 1–9.

DOWNES, H. 1985. Evidence for magma heterogeneity in the White River ash (Yukon Territory). Canadian Journal of Earth Sciences 22:929–934.

DUGMORE, A.J. 1989. Icelandic volcanic ash in Scotland. Scottish Geographical Magazine 105:168–172.

DUGMORE, A.J., NEWTON, A.J., SUGDEN, D.E., and LARSEN, G. 1992. Geochemical stability of fine-grained silicic Holocene tephra in Iceland and Scotland. Journal of Quaternary Science 7:173–183.

DUGMORE, A.J., NEWTON, A.J., EDWARDS, K.J., LARSEN, G., BLACKFORD, J.J., and COOK, G.T. 1996. Long-distance marker horizons from small-scale eruptions: British tephra deposits from the AD 1510 eruption of Hekla, Iceland. Journal of Quaternary Science 11:511–516.

HALL, V., and PILCHER, J. 2002. Late-Quaternary Icelandic tephras in Ireland and Great Britain: Detection, characterization and usefulness. The Holocene 12:223–230.

HUNT, J.B. 2004. Tephrostratigraphical evidence for the timing of Pleistocene explosive volcanism at Jan Mayen. Journal of Quaternary Science 19:121–136.

HUNT, J.B., and HILL, P.G. 1993. Tephra geochemistry: A discussion of some persistent analytical problems. The Holocene 3:271–278.

HUNT, J.B., CLIFT, P.D., LACASSE, C., VALLIER, T.L., and WERNER, R. 1998. Interlaboratory comparison of electron probe microanalysis of glass geochemistry. In: Saunders, A.D., Larsen, H.C., and Wise, S.W., eds. Proceedings of the Ocean Drilling Program, Scientific Results, Vol. 152:85–92, doi:10.2973/odp.proc.sr.152.244.1998. College Station, Texas: ODP, Texas A&M University.

LOWE, D.J., and HUNT, J.B. 2001. A summary of terminology used in tephra-related studies. In: Juvigné, E., and Raynal, J.-P., eds. Tephra: Chronology, archaeology. Les Dossiers de l'Archéo-Logis 1:17–22.

PAYNE, R.J., and BLACKFORD, J.J. 2004. Distal micro-tephra deposits in southeast Alaskan peatlands, In: Emond, D.S., and Lewis, L.L., eds. Yukon exploration and geology 2003. Whitehorse: Yukon Geological Survey. 191–197.

PAYNE, R.J., KILFEATHER, A., VAN DER MEER, J., and BLACKFORD, J.J. 2005. Experiments on the taphonomy of tephra in peatlands. Suo 56:147–156.

PAYNE, R.J., KISHABA, K., BLACKFORD, J.J., and MITCHELL, E.A.D. 2006. The ecology of testate amoebae (Protists) in south-central Alaska peatlands: Building transfer function models for palaeoenvironmental studies. The Holocene 16:403–414.

PERSSON, C. 1971. Tephrochronological investigations of peat deposits in Scandinavia and on the Faroe Islands. Sveriges Geologiska Undersökning 65:3–34.

PILCHER, J.R., and HALL, V.A. 1992. Towards a tephrochronology for the Holocene of the north of Ireland. The Holocene 2: 255–259, doi:10.1177/095968369200200307.

RICHTER, D.H., PREECE, S.J., McGIMSEY, R.G., and WESTGATE, J.A. 1995. Mount Churchill, Alaska: Source of the late Holocene White River Ash. Canadian Journal of Earth Sciences 32:741–748.

RIEHLE, J.R. 1985. A reconnaissance of the major Holocene tephra deposits in the upper Cook Inlet, Alaska. Journal of Volcanology and Geothermal Research 26:37–54.

RIEHLE, J.R., MEYER, C.E., AGER, T.A., KAUFMAN, D.S., and ACKERMAN, R.E. 1987. The Aniakchak tephra deposit, a late Holocene marker horizon in western Alaska. U.S. Geological Survey Circular 998:19–22.

RIEHLE, J.R., BOWERS, P.M., and AGER, T.A. 1990. The Hayes tephra deposits, an upper Holocene marker horizon in south-central Alaska. Quaternary Research 33:276–290.

RIEHLE, J.R., MANN, D.H., PETEET, D.M., ENGSTROM, D.R., BREW, D.A., and MEYER, C.E. 1992. The Mount Edgecumbe tephra deposits, a marker horizon in southeastern Alaska near the Pleistocene-Holocene boundary. Quaternary Research 37:183–202, doi:10.1016/0033-5894(92)90081-S.

RIEHLE, J.R., MEYER, C.E., and MIYAOKA, R.T. 1999. Data on Holocene tephra (volcanic ash) deposits in the Alaska Peninsula and lower Cook Inlet region of the Aleutian volcanic arc, Alaska. US Geological Survey, Open-File Report 99-135.

ROBINSON, S.D., and MOORE, T.R. 1999. Carbon and peat accumulation over the past 1200 years in a landscape with discontinuous permafrost, northwestern Canada. Global Biogeochemical Cycles 13:591–601.

RODBELL, D.T., BAGNATO, S., NEBOLINI, J.C., SELTZER, G.O., and ABBOTT, M.B. 2002. A late Glacial–Holocene tephrochronology for glacial lakes in southern Ecuador. Quaternary Research 57:343–354, doi:10.1006/qres2002.2324.

APPENDIX

Electron microprobe data. Results as raw percentages from Bergen (B) and Edinburgh (E) microprobes. Averages of raw and normalized data and standard deviation are also shown.

ST 12	E	E	E	E	E	E	E	E	E	E	E	E	E	E	E
SiO_2	74.50	71.50	74.84	75.25	75.34	74.81	74.56	76.53	75.17	74.93	74.32	74.01	73.25	74.14	74.80
TiO_2	0.41	0.29	0.34	0.29	0.40	0.43	0.31	0.40	0.30	0.43	0.42	0.39	0.37	0.38	0.28
Al_2O_3	12.66	15.68	12.43	12.48	11.92	12.29	12.32	11.22	11.87	12.34	12.17	12.72	12.60	12.40	12.32
FeO	2.16	1.50	1.85	1.83	2.03	1.80	1.99	1.57	1.98	1.92	2.05	1.73	2.22	2.04	1.76
MnO	0.05	0.00	0.08	0.00	0.11	0.03	0.08	0.13	0.00	0.03	0.10	0.03	0.06	0.08	0.08
MgO	0.52	0.19	0.48	0.36	0.36	0.43	0.49	0.23	0.43	0.40	0.48	0.26	0.65	0.44	0.41
CaO	2.18	3.20	1.93	1.87	1.94	1.91	1.98	1.04	1.79	1.90	1.99	2.04	2.37	1.82	1.79
Na_2O	4.28	5.06	4.34	4.23	3.99	4.33	4.33	4.10	4.26	4.03	4.33	4.60	4.34	4.40	4.18
K_2O	2.25	1.55	2.10	2.06	2.24	2.16	2.03	2.84	2.26	2.03	2.13	2.10	1.98	2.09	2.18
	99.01	98.96	98.40	98.38	98.34	98.19	98.07	98.06	98.05	98.01	97.99	97.89	97.84	97.80	97.80

ST 12 - continued	E	E	E	E	E	E	E	E	E	E	E	E	E	E	E	Mean	Mean norm.	SD
SiO_2	74.46	74.86	74.12	74.46	76.39	73.18	73.87	74.77	74.10	73.17	73.09	73.87	73.10	73.81	72.61	74.26	76.25	1.07
TiO_2	0.25	0.11	0.35	0.33	0.47	0.30	0.34	0.43	0.34	0.32	0.34	0.43	0.31	0.37	0.30	0.35	0.36	0.07
Al_2O_3	12.61	12.23	12.53	12.04	11.00	12.54	12.62	12.10	12.70	12.24	12.82	11.29	12.08	12.32	12.18	12.36	12.69	0.75
FeO	2.02	1.88	1.73	2.00	1.97	2.09	2.10	1.82	1.82	1.86	1.68	2.08	1.95	2.02	1.74	1.91	1.96	0.18
MnO	0.01	0.05	0.03	0.12	0.05	0.08	0.08	0.12	0.09	0.04	0.10	0.02	0.05	0.08	0.06	0.06	0.06	0.04
MgO	0.53	0.40	0.41	0.42	0.33	0.48	0.55	0.40	0.35	0.38	0.39	0.46	0.42	0.39	0.38	0.41	0.43	0.10
CaO	2.18	1.94	1.93	2.01	1.47	2.05	2.12	1.84	2.21	2.00	2.34	1.62	1.73	1.82	1.87	1.96	2.01	0.35
Na_2O	3.34	4.10	4.18	3.40	3.14	4.26	3.19	3.07	2.93	4.12	3.24	3.97	4.07	2.81	4.19	3.96	4.06	0.54
K_2O	2.29	2.07	2.03	2.46	2.26	2.10	2.03	2.10	1.85	2.06	1.96	2.16	2.11	2.12	2.05	2.12	2.18	0.21
	97.68	97.63	97.30	97.22	97.08	97.08	96.89	96.66	96.37	96.19	95.96	95.90	95.83	95.74	95.37	97.39		

ST 24	E	E	E	E	E	E	E	E	E	E	E	E	E	E	Mean	Mean norm.	SD
SiO_2	74.55	70.77	77.28	75.22	74.36	72.54	73.11	76.86	74.05	73.90	72.45	73.43	74.74	73.94	74.08	76.86	1.89
TiO_2	0.44	0.42	0.21	0.17	0.24	0.30	0.32	0.24	0.23	0.30	0.28	0.38	0.23	0.33	0.29	0.30	0.08
Al_2O_3	13.74	14.03	11.11	11.77	12.05	12.98	12.28	11.43	11.82	11.35	12.79	11.95	11.63	11.82	12.20	12.65	0.83
FeO	1.83	1.80	1.27	0.93	1.82	1.54	1.80	1.01	1.03	1.20	1.61	1.85	1.07	1.25	1.43	1.48	0.36
MnO	0.09	0.07	0.00	0.03	0.05	0.09	0.00	0.05	0.04	0.08	0.07	0.04	0.00	0.07	0.05	0.05	0.03
MgO	0.41	0.53	0.18	0.22	0.40	0.38	0.38	0.12	0.26	0.24	0.38	0.42	0.19	0.23	0.31	0.32	0.12
CaO	1.75	1.84	1.32	1.09	1.63	1.69	2.00	0.58	1.07	0.97	1.80	1.95	1.10	1.14	1.42	1.48	0.45
Na_2O	3.03	5.05	2.75	4.27	4.07	4.15	4.53	2.95	4.02	4.24	3.18	3.26	3.22	3.11	3.70	3.84	0.73
K_2O	3.07	3.06	3.06	3.24	2.21	3.02	2.16	3.10	3.15	3.33	2.93	2.12	3.16	3.14	2.91	3.02	0.43
	98.91	97.58	97.18	96.94	96.83	96.69	96.58	96.35	95.68	95.62	95.49	95.39	95.34	95.03	96.40		

ST 36	E	E	E	E	E	E	E	E	E	E	E	E	E	E	E	E	Mean	Mean norm.	SD
SiO_2	70.49	72.13	73.17	73.26	72.48	73.76	74.56	69.38	72.14	72.47	72.79	72.80	75.91	72.92	72.05	72.01	72.65	75.08	1.95
TiO_2	0.44	0.40	0.41	0.53	0.49	0.48	0.39	0.67	0.43	0.43	0.50	0.68	0.52	0.50	0.35	0.40	0.48	0.49	0.10
Al_2O_3	15.30	14.96	13.23	12.49	13.13	11.93	12.18	14.08	13.09	12.78	13.05	12.17	10.93	12.50	12.55	12.37	12.92	13.34	1.02
FeO	1.87	2.04	2.51	2.05	2.64	2.15	1.99	3.25	2.46	2.51	2.15	2.59	1.69	2.00	2.22	2.05	2.26	2.33	0.40
MnO	0.13	0.13	0.07	0.05	0.10	0.10	0.00	0.11	0.07	0.08	0.07	0.00	0.01	0.07	0.05	0.07	0.07	0.07	0.04
MgO	0.59	0.43	0.60	0.50	0.73	0.49	0.49	0.95	0.61	0.68	0.48	0.55	0.29	0.48	0.54	0.55	0.56	0.58	0.15
CaO	3.29	3.23	2.44	2.28	2.78	2.09	2.10	3.32	2.74	2.61	2.37	2.52	1.33	2.32	2.42	2.60	2.53	2.61	0.50
Na_2O	5.03	3.70	3.04	4.28	3.13	4.01	3.22	3.19	3.26	3.16	3.10	2.78	2.84	2.95	2.99	3.01	3.35	3.46	0.59
K_2O	2.13	1.82	1.99	1.97	1.88	1.93	1.88	1.81	1.91	1.93	1.92	1.99	2.37	1.93	1.96	1.98	1.96	2.03	0.14
	99.27	98.83	97.46	97.40	97.36	96.94	96.81	96.75	96.70	96.63	96.44	96.09	95.89	95.65	95.13	95.05	96.78		

ST68	E	E	E	E	E	E	E	E	E	E	E	E	E	Mean	Mean norm.	SD
SiO_2	76.26	72.26	74.07	73.98	72.75	75.70	71.79	73.81	74.23	75.00	74.33	70.57	71.22	73.54	74.94	1.73
TiO_2	0.20	0.21	0.10	0.26	0.23	0.21	0.25	0.14	0.25	0.22	0.24	0.16	0.26	0.21	0.21	0.05
Al_2O_3	15.03	18.35	14.59	13.34	12.49	12.32	13.81	13.02	13.33	11.80	12.98	15.54	13.73	13.87	14.12	1.60
FeO	1.87	0.91	1.00	1.44	2.57	1.04	2.11	1.02	1.10	1.19	1.18	0.95	1.16	1.35	1.37	0.52
MnO	0.12	0.08	0.01	0.09	0.14	0.12	0.15	0.08	0.05	0.07	0.01	0.03	0.04	0.08	0.08	0.05
MgO	0.43	0.16	0.36	0.31	1.77	0.15	1.24	0.21	0.23	0.16	0.19	0.17	0.37	0.44	0.45	0.50
CaO	1.96	4.11	2.38	2.10	2.75	1.50	1.93	1.94	1.99	1.43	1.65	3.26	2.14	2.24	2.28	0.74
Na_2O	3.48	3.30	4.57	4.24	2.82	3.28	3.78	4.29	3.37	3.73	3.76	4.10	4.16	3.76	3.84	0.53
K_2O	2.31	1.64	2.37	2.47	2.60	3.60	2.44	2.84	2.71	3.48	2.70	2.00	3.36	2.65	2.71	0.60
	101.6	101.0	99.45	98.22	98.11	97.91	97.51	97.35	97.26	97.08	97.06	96.77	96.43	98.14		

MP10: Population A

	B	B	B	B	B	B	E	E	E	E	E	E	E	E	E	E	E	Mean	Mean norm.	SD
SiO_2	75.30	74.38	72.11	73.15	71.17	71.90	76.81	76.53	74.36	71.81	73.13	72.95	76.05	71.08	72.41	73.85	70.19	73.36	75.61	1.41
TiO_2	0.34	0.25	0.40	0.32	0.36	0.26	0.18	0.24	0.24	0.43	0.29	0.31	0.17	0.38	0.40	0.32	0.30	0.31	0.31	0.08
Al_2O_3	13.66	13.40	13.55	13.22	13.53	12.99	12.33	12.55	13.41	14.04	13.20	13.25	12.36	14.19	12.51	11.98	13.09	13.13	13.54	0.66
FeO	1.61	1.65	1.56	1.62	1.61	1.53	0.88	1.22	1.57	2.26	1.82	1.58	1.16	1.95	1.96	1.69	1.80	1.62	1.67	0.34
MnO	0.09	0.07	0.02	0.07	0.06	0.09	0.09	0.07	0.05	0.07	0.11	0.13	0.04	0.07	0.00	0.08	0.06	0.07	0.07	0.03
MgO	0.44	0.39	0.34	0.43	0.36	0.30	0.23	0.26	0.35	0.56	0.32	0.44	0.22	0.61	0.39	0.31	0.56	0.38	0.39	0.12
CaO	1.90	1.88	1.65	1.88	1.72	1.81	1.05	1.31	1.69	2.29	1.45	1.97	1.13	2.22	1.64	1.37	1.75	1.69	1.74	0.36
Na_2O	2.76	3.61	3.80	2.50	3.56	3.34	4.03	3.40	3.07	3.21	4.95	2.99	2.46	3.34	4.37	3.88	4.36	3.51	3.62	0.71
K_2O	3.02	2.91	2.97	2.76	2.90	2.87	3.32	3.14	3.10	2.76	2.10	3.09	3.15	2.79	2.83	2.87	2.81	2.91	2.99	0.26
	99.13	98.54	96.38	95.95	95.28	95.09	98.93	98.77	97.89	97.59	97.47	96.82	96.81	96.76	96.56	96.44	95.02	97.02		

MP10: Population B

	B	B	B	B	B	E	E	E	E	E	E	E	E	E	E	E	E	E	E	E	E	Mean	Mean norm.	SD
SiO_2	68.13	69.38	67.30	68.85	68.05	69.99	68.29	68.60	66.70	68.61	68.47	67.40	66.62	66.74	69.19	65.28	67.77	67.08	67.25	65.75	65.63	65.69	67.58	69.02	1.02
TiO_2	0.48	0.47	0.48	0.30	0.39	0.52	0.51	0.61	0.49	0.53	0.50	0.51	0.56	0.49	0.54	0.75	0.49	0.48	0.46	0.48	0.57	0.57	0.51	0.52	0.09
Al_2O_3	14.44	15.43	14.29	10.96	15.36	16.45	16.11	15.73	16.62	15.96	15.28	16.09	15.15	16.06	15.18	14.79	15.05	14.89	15.20	15.33	15.02	14.75	15.19	15.51	1.10
FeO	3.90	2.87	4.26	5.02	2.91	2.99	3.38	3.55	3.18	2.84	3.28	3.35	3.39	3.16	2.67	5.86	3.54	3.47	3.32	3.89	3.40	3.80	3.55	3.62	0.76
MnO	0.21	0.13	0.19	0.27	0.13	0.17	0.07	0.11	0.22	0.04	0.13	0.06	0.12	0.12	0.13	0.04	0.13	0.13	0.09	0.10	0.12	0.15	0.13	0.13	0.06
MgO	2.86	0.98	3.47	5.42	0.96	1.23	1.18	1.27	1.04	0.68	1.06	1.04	1.18	1.09	0.57	0.82	1.10	1.17	1.04	1.30	1.17	1.23	1.45	1.48	1.13
CaO	2.93	3.02	2.88	1.77	3.03	3.34	3.31	3.03	4.24	3.26	3.35	3.73	3.49	3.68	3.01	2.88	3.21	3.37	3.67	3.31	3.28	3.74	3.25	3.32	0.49
Na_2O	3.74	2.98	2.34	2.67	4.00	4.43	3.68	3.62	3.71	3.93	3.83	3.42	4.77	3.90	3.71	4.61	3.40	3.41	3.13	3.65	4.59	3.46	3.68	3.76	0.61
K_2O	2.33	2.50	2.35	2.27	2.57	2.52	2.54	2.48	2.21	2.41	2.32	2.17	2.37	2.36	2.50	2.30	2.60	2.55	2.27	2.52	2.34	2.32	2.40	2.45	0.13
	99.03	97.75	97.54	97.52	97.39	101.8	99.37	99.23	98.65	98.56	98.44	98.02	97.85	97.84	97.71	97.62	97.53	96.81	96.65	96.53	96.38	95.93	97.92		

MP27 Population A Population B

	B	B	B	B	B	B	B	B	B	B	B	Mean	Mean norm.	SD
SiO_2	60.88	59.33	58.23	59.19	58.56	60.31	58.94	58.57	58.96	59.56	60.82	59.39	59.74	1.03
TiO_2	1.08	1.21	1.26	1.12	1.10	1.15	1.21	1.13	1.20	1.10	0.95	1.14	1.14	0.08
Al_2O_3	16.64	16.73	16.50	16.46	16.46	16.28	16.28	16.32	16.12	15.99	16.28	16.37	16.46	0.14
FeO	7.30	7.95	8.48	8.21	8.12	7.41	8.08	8.15	7.81	7.48	6.42	7.77	7.81	0.56
MnO	0.21	0.16	0.19	0.18	0.16	0.22	0.20	0.21	0.15	0.19	0.24	0.19	0.19	0.03
MgO	2.55	2.94	3.13	2.95	2.98	2.74	2.78	2.89	2.84	2.51	2.09	2.76	2.78	0.28
CaO	6.02	6.33	6.58	6.45	6.51	5.77	6.37	6.47	6.66	5.85	5.42	6.22	6.25	0.39
Na_2O	4.21	3.85	3.80	3.56	4.10	3.95	3.94	3.96	3.98	4.19	4.13	3.97	3.99	0.20
K_2O	1.69	1.56	1.61	1.64	1.56	1.65	1.58	1.61	1.29	1.75	1.86	1.62	1.63	0.15
	100.6	100.1	99.77	99.76	99.55	99.47	99.38	99.30	99.00	98.61	98.20	99.42		

MP 39

	B	B	B	B	B	B	B	B	B	B	B	B	B	B	B	B	B	B	B
SiO_2	70.24	66.44	61.73	60.83	60.61	59.04	59.37	57.64	57.24	58.77	60.13	56.78	58.35	56.01	56.35	58.23	56.75	58.60	56.81
TiO_2	0.76	0.90	1.19	1.10	1.15	1.00	1.58	1.23	1.22	1.19	1.16	1.25	1.20	1.11	1.07	1.14	1.17	1.11	1.10
Al_2O_3	15.17	14.31	15.95	16.10	16.18	16.26	14.69	16.31	16.27	15.84	15.87	15.88	15.56	16.20	15.87	15.50	14.73	15.35	15.50
FeO	3.22	4.57	7.04	7.23	7.23	7.66	8.92	7.91	8.31	7.47	6.68	8.27	7.41	7.92	8.05	7.17	8.20	6.80	7.64
MnO	0.21	0.26	0.19	0.18	0.21	0.27	0.25	0.26	0.22	0.23	0.16	0.20	0.16	0.18	0.23	0.26	0.24	0.17	0.20
MgO	0.80	0.84	2.48	2.48	2.51	2.95	2.46	3.10	3.00	2.68	2.29	3.13	2.65	2.95	2.87	2.42	2.87	2.37	2.91
CaO	2.37	2.65	5.68	5.80	5.65	6.29	5.37	6.38	6.59	5.87	5.39	6.64	5.95	6.65	6.53	5.75	6.46	5.31	6.21
Na_2O	4.01	3.92	3.84	4.17	3.81	3.95	3.65	3.80	3.77	3.99	3.81	3.71	3.66	3.91	3.49	3.76	3.58	3.98	3.34
K_2O	2.94	2.75	1.89	1.88	1.79	1.59	2.04	1.63	1.60	1.68	1.89	1.43	1.61	1.42	1.56	1.67	1.53	1.83	1.49
	99.73	96.62	99.99	99.75	99.14	99.01	98.34	98.24	98.21	97.71	97.38	97.28	96.54	96.34	96.02	95.92	95.52	95.52	95.20

MP 39 – continued

	E	E	E	E	E	E	E	E	E	E	E	E	E	E	E	E	E	E	E
SiO_2	68.74	64.41	64.31	62.10	61.17	60.76	60.37	59.78	59.45	59.41	59.39	59.39	59.26	58.62	58.59	58.55	58.29	58.13	58.11
TiO_2	0.70	0.85	0.61	0.90	1.24	1.03	1.04	1.03	1.02	1.08	1.17	1.13	1.07	1.12	1.16	0.98	1.22	1.07	1.16
Al_2O_3	14.81	14.71	14.81	15.53	14.99	15.68	15.54	15.89	15.49	15.85	16.19	15.87	15.58	15.53	15.90	15.57	15.18	15.45	16.06
FeO	3.68	5.12	5.65	5.40	6.86	6.69	6.58	7.47	6.94	7.28	7.31	7.54	7.60	7.60	7.46	7.31	7.57	7.71	8.32
MnO	0.17	0.19	0.06	0.19	0.21	0.35	0.13	0.23	0.23	0.23	0.16	0.26	0.19	0.20	0.28	0.19	0.20	0.22	0.19
MgO	0.83	1.62	1.75	1.82	2.10	2.31	2.37	2.67	2.40	2.54	2.59	2.63	2.75	2.72	2.71	2.68	2.91	2.65	2.85
CaO	2.34	3.75	4.42	4.36	4.60	5.01	5.14	5.65	5.51	5.54	5.58	5.73	5.74	5.91	6.07	5.65	6.33	6.00	6.38
Na_2O	5.21	4.91	4.61	4.96	4.47	4.58	4.59	4.23	4.38	4.20	4.32	4.37	4.43	4.26	4.45	4.40	3.80	4.31	4.09
K_2O	2.89	2.41	2.06	2.06	2.00	1.98	1.90	1.71	1.85	1.69	1.82	1.69	1.71	1.72	1.77	1.74	1.35	1.55	1.69
	99.49	98.19	98.42	97.72	98.13	98.66	97.96	98.95	97.58	98.09	98.83	98.91	98.72	97.94	98.73	97.33	97.20	97.37	99.19

MP 39 – continued

	E	E	E	E	E	E	E	E	E	E	E	E	E	E	E	E	E	E	E	E	Mean	Mean norm.	SD
SiO_2	58.06	58.00	57.95	57.68	57.60	57.47	57.46	57.44	57.19	57.17	57.07	57.06	56.98	56.98	56.82	56.78	56.42	56.27	55.89	55.84	58.98	60.32	2.71
TiO_2	1.17	1.17	1.14	1.13	1.14	1.19	1.15	1.15	1.14	1.22	1.11	1.29	1.14	1.23	1.19	1.23	1.09	1.13	1.17	1.12	1.11	1.14	0.15
Al_2O_3	15.59	16.17	15.88	15.97	15.80	15.75	15.96	15.97	15.61	15.86	15.88	15.15	15.47	15.56	15.59	15.69	15.82	15.46	15.54	15.06	15.62	15.98	0.44
FeO	7.14	7.76	7.83	8.59	7.73	8.26	7.86	8.04	7.42	7.93	8.24	8.25	8.04	8.11	8.18	8.82	7.48	8.26	8.14	7.73	7.37	7.54	1.15
MnO	0.20	0.19	0.24	0.20	0.21	0.21	0.13	0.27	0.23	0.21	0.24	0.21	0.11	0.16	0.18	0.27	0.22	0.19	0.25	0.27	0.21	0.21	0.05
MgO	2.74	2.79	2.92	3.08	2.94	2.95	3.03	3.11	2.80	3.04	2.98	2.73	2.95	3.01	2.97	3.13	2.73	3.04	2.90	2.89	2.61	2.67	0.55
CaO	5.92	6.17	6.20	6.64	6.51	6.51	6.28	6.51	5.99	6.57	6.54	5.80	6.54	6.31	6.57	6.75	6.04	6.46	6.41	7.88	5.79	5.93	1.08
Na_2O	4.33	4.16	4.25	4.28	4.01	4.06	4.05	4.00	4.27	4.27	4.04	4.32	4.36	4.03	4.11	3.76	4.13	3.93	3.89	3.70	4.11	4.21	0.35
K_2O	1.69	1.69	1.44	1.56	1.44	1.65	1.59	1.38	1.50	1.47	1.51	1.91	1.54	1.71	1.47	1.39	1.71	1.51	1.34	1.44	1.74	1.77	0.34
	97.27	98.40	98.22	99.46	97.74	98.38	97.83	98.21	96.45	98.10	97.96	97.11	97.52	97.46	97.42	98.22	96.00	96.59	95.84	96.24	97.76		